Cycloheptatrienyl-Bridged Triple-Decker Complexes

Adrian Hauser,[▽] Luca Münzfeld,[▽] Sören Schlittenhardt, Cedric Uhlmann, Louis Leyen, Eufemio Moreno-Pineda, Mario Ruben, and Peter W. Roesky*

ABSTRACT: The first structurally characterized organometallic multidecker sandwich complexes featuring a cycloheptatrienyl ring (Cht, $C_7H_7^{3-}$) in the coordination sphere are presented. The synthesis of inverse sandwich complexes of the rare earth elements Y^{III} and Er^{III} with a bridging cycloheptatrienyl ligand of the type $[(thf)(BH_4)_2Ln^{III}(\mu-\eta^7:\eta^7\text{-Cht})Ln^{III}(BH_4)(thf)_2]$ is described first. The subsequent introduction of the Cot^{TIPS} ligand (Cot^{TIPS} = 1,4-($^iPr_3Si)_2C_8H_6^{2-}$) into the coordination sphere of the rare earth cations resulted in the isolation of unprecedented triple-decker compounds with the formula $[(thf)_3K\{(\eta^8\text{-}Cot^{TIPS})\text{-}Ln^{III}\}_2(\mu-\eta^7:\eta^7\text{-Cht})]$, bearing a seven-membered aromatic carbon ring as a middle deck. These compounds are also the first examples of rare earth triple-decker complexes not bridged by a Cot derivative, based on purely carbon-based ligands. The magnetic properties of the respective Er^{III} congeners were investigated in detail, leading to the observation of antiferromagnetic coupling of the Er^{III} cations and a blocking temperature of 13.5 K. The conversion of the Y^{III} compound $[(thf)_3K\{(\eta^8\text{-}Cot^{TIPS})Y^{III}\}_2(\mu-\eta^7:\eta^7\text{-Cht})]$ with $[Y^{III}(Cot)I(thf)_2]$ resulted in ligand rearrangement and the selective formation of the first triple-decker complex ($[(\eta^8\text{-}Cot^{TIPS}Y^{III})_2(\mu-\eta^8:\eta^8\text{-Cot})]$) featuring two Cot ligands with different substituents in its coordination sphere.

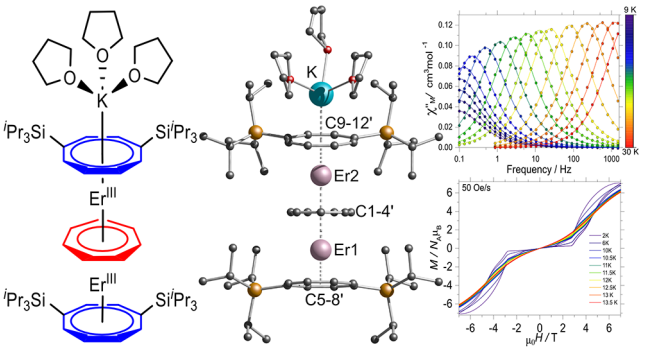

INTRODUCTION

One fundamental class of compounds in organometallic chemistry are sandwich compounds, in which the central metal ion is coordinated by two planar, aromatic, and cyclic ligand systems. If the ligands are two Cp units (Cp = cyclopentadienyl), they are classically referred to as metallocenes.[1] In the field of f-element chemistry, sandwich compounds with larger cyclic ligands such as cyclooctatetraendiide (Cot^{2-}) of the form $[(\eta^8\text{-Cot})_2Ln^{III/IV}]^{-/0}$ and recently also cyclononatetraenyl-anion (Cnt^-) $[(\eta^9\text{-Cnt})_2Ln^{II}]$ are well established.[2−6] In addition to these homoleptic compounds, heteroleptic lanthanide sandwich compounds with mixed ring sizes such as $[(\eta^8\text{-Cot})Ln(\eta^5\text{-}C_5Me_5)]$ or $[(\eta^8\text{-Cot})Ln(Cnt)]$ are also well investigated.[7−12] In recent years, research has focused on not only simple sandwich compounds with different aromatic ring systems as ligands but also multidecker compounds, which are larger stacks of metal ions and planar aromatic rings.[13−21] The structural motif for this class of compounds is the homoleptic Cot-based $[Ln_2^{III}(Cot'')_3]$ (Cot" = 1,4-$(Me_3Si)_2C_8H_6^{2-}$) (Ln = Y, La, Ce, Nd, Sm, Tb, Dy, Ho, Er, Tm, Lu) triple-decker complexes,[15,16,22−25] the even larger mixed-valent quadruple decker compound $[Sm_3^{III/II/III}(Cot^{TIPS})_4]$ (Cot^{TIPS} = 1,4-($^iPr_3Si)_2C_8H_6^{2-}$), the solvates $[Ln_2(Cot)_3(THF)_2]$,[14,26] and the heteroleptic quadruple decker complex $[Cp^*_2Yb_3^{II}(Cot''')_2]$ (Cp^* = $C_5Me_5^-$) (Cot''' = 1,3,6-$(Me_3Si)_3C_8H_5^{2-}$).[18,20] Recently, also, cyclic nanometer-scale sandwich complexes (cyclocenes) consisting of 18 repeating units, forming almost ideally circular, closed rings in the solid state $[cyclo\text{-}M^{II}(\mu-\eta^8:\eta^8\text{-}Cot^{TIPS})]_{18}$, were disclosed.[27] It is noteworthy that for purely carbon-based aromatic ring systems, the bridging units of these compounds consist exclusively of Cot and its derivatives, while the outer ligands vary. Therefore, our efforts were aimed at synthesizing the first multidecker complexes with a ring size other than eight in the center. As the target ligand, we aimed for the cycloheptatrienyl trianion ($C_7H_7^{3-}$, Cht) as the middle deck, to learn about the communications of the metals through the deck. The first reports of the formation of the cycloheptatrienyl trianion ($C_7H_7^{3-}$, Cht) from lithium cycloheptadienyl ($[Li(C_7H_9)]$), in the presence of lanthanide and actinide chlorides, date back to 1981.[28] Fundamental insights and crystallographic evidence of the trianionic Cht ligand in the field of f-elements were first described by Ephritikhine et al. in the 1990s with the synthesis of a homoleptic $[K(18\text{-crown-}6)][U(\eta^7\text{-}C_7H_7)_2]$ and inverse

sandwich compounds of uranium and neodymium.[29−32] The inverse sandwich complex [(thf)$(BH_4)_2Nd^{III}(\mu-\eta^7:\eta^7$-Cht)-$Nd^{III}(BH_4)(thf)_3$] (Figure 1, **I**) was for a long time considered

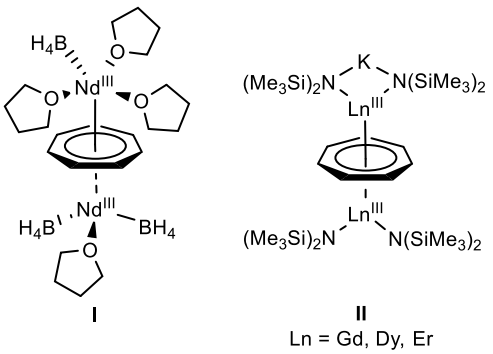

Figure 1. Structural examples of inverse Cht sandwich complexes of rare earth elements.[30,34]

to be the only example of a Ln^{III} compound with a bridging Cht unit.[30,33] It was not until 20 years after its synthesis that the structurally related compounds [$KLn_2^{III}(\mu-\eta^7:\eta^7$-Cht)$(N(SiMe_3)_2)_4$] (Figure 1, **II**) (Ln = Dy, Gd, Er) could be isolated and their magnetic properties as well as the exchange interactions of the lanthanides across the seven-membered ring were investigated.[34] In these compounds, η^7-Cht was found to efficiently promote ferromagnetic exchange interactions between metal ions. Despite this pioneering work, the two structural examples described, in which the seven-membered ring exists exclusively as a trianionic 10π-aromatic system, remain the only ones for rare earth metals to this day. In contrast, Cht complexes of the d-metals are well established. Most prominent in this series are the mixed sandwich complexes [$(\eta^7$-$C_7H_7)M(\eta^5$-$C_5H_5)$] (M = Ti, Zr, Hf, V, Ta, Cr, Mo). They are also referred to as, e.g., troticene (M = Ti, derived from tropylium titanium cyclopentadienyl), trozircene (M = Zr), trohafcene (M = Hf), trovacene (M = V), and trochrocene (M = Cr).[35−40] Furthermore, Cht sandwich complexes with heterocycles of the general formula [$(\eta^7$-$C_7H_7)Zr(L)$] (L = phospholyl, boratabenzene) are known.[41−43] In general, the seven-membered aromatic ring in compounds of the later transition metals is formulated monocationically, and a covalent bond between the metal and ligand is observed. For the earlier transition metals, both experimental findings and density functional theory (DFT) calculations support the assumption of a trianionic ligand.[33,36,44] Besides the synthetic challenges, sandwich complexes of lanthanides have also been intensively investigated in terms of their properties as single-molecule magnets (SMMs). The synthesis strategies for organometallic Er^{III} SMMs with carbon-based aromatic ligands are often focused on the use of the Cot ligand and its derivatives.[23,45−49] This is attributable to the properties of the eight-membered ring. Its equatorial ligand field preferentially stabilizes the prolate m_J = 15/2 state of Er^{III} ions.[49,50]

On the other hand, it was shown that significant exchange coupling occurred in [$KLn_2^{III}(\mu-\eta^7:\eta^7$-Cht)$(N(SiMe_3)_2)_4$] (Ln = Dy, Gd, Er) due to the Cht bridging ligand.[34] Therefore, to optimize the magnetic properties of the target compound, the outer decks of the anticipated multidecker complex should consist of Cot derivatives capable of stabilizing the anisotropy of the Er^{III} ions in addition to the bridging Cht ligand, which allows exchange coupling. Herein, we report on the first structurally characterized multidecker sandwich complex in organometallic chemistry featuring a cycloheptatrienyl ring in the coordination sphere. Besides the synthesis, we also investigated the structural and magnetic properties of the new compounds.

RESULTS AND DISCUSSION

Focusing on the target of synthesizing lanthanide-based Cht-bridged heteroleptic multidecker complexes, we first aimed for the synthesis of lanthanide compounds with an inverse sandwich structural motif [$(thf)(BH_4)_2Ln^{III}(\mu-\eta^7:\eta^7$-Cht)-$Ln^{III}(BH_4)(thf)_2$] (**1-Ln**, Scheme 1).[51] Here, we followed a route established by Ephritikhine et al. for the analogous Nd^{III}-compound.[30] For this purpose, 3 equiv of [$K(C_7H_9)$] was reacted with 2 equiv of the respective Ln^{III}-borohydride precursor [$Ln^{III}(BH_4)_3(thf)_3$] (Ln = Y, Er). The in situ disproportionation of [$K(C_7H_9)$] in this process leads to the formation of 2 equiv of cycloheptadiene (C_7H_{10}) and 1 equiv of [$K_3(C_7H_7)$], which subsequently reacts with [$Ln^{III}(BH_4)_3(thf)_3$] (Ln = Y, Er) to produce the inverse sandwich compounds [$(thf)(BH_4)_2Ln^{III}(\mu-\eta^7:\eta^7$-Cht)-

Scheme 1. Synthesis of the Inverse Sandwich Compounds 1-Ln, Subsequent Functionalization to form the Heteroleptic Triple-Decker Compounds 2-Ln, and Consecutive Reaction to the Homoleptic Triple-Decker Complex 3[a]

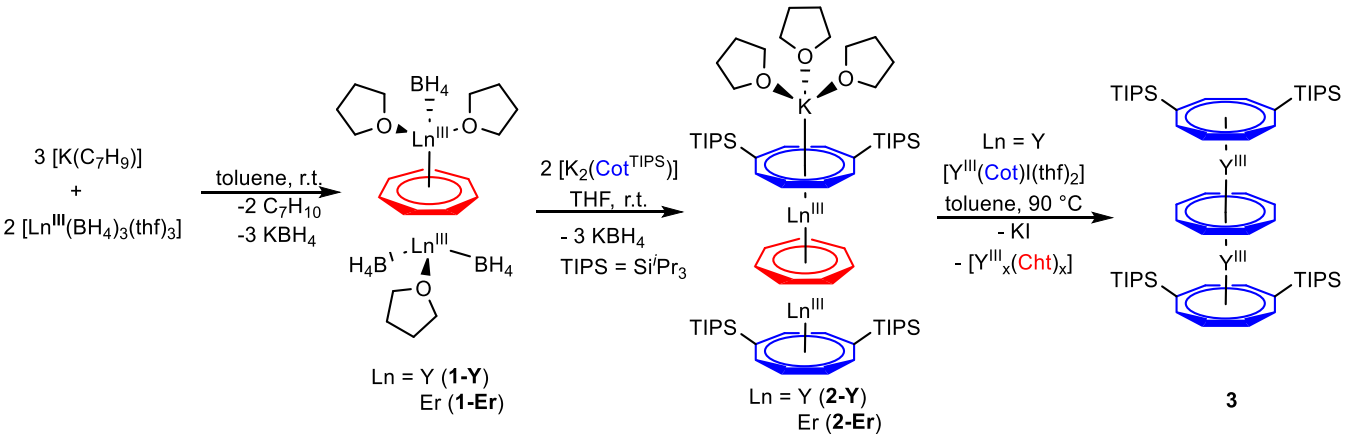

[a]Red: Seven-membered Cht-ring $(C_7H_7)^{3-}$; blue: eight-membered Cot-ring $(C_8H_6R_2)^{2-}$ (R = H or TIPS).

$Ln^{III}(BH_4)(thf)_2]$ (**1-Ln**) (Ln = Y, Er) (Scheme 1).[30,33] The isomorphic compounds **1-Ln** crystallize in the monoclinic space group $P2_1/c$ with one coordinating THF molecule less compared to the reported Nd^{III} analogue.[30] The reason for this is most likely the increased ionic radius of Nd^{III} compared to Y^{III} and Er^{III}.[52] Both Ln^{III} cations are present in a piano chair coordination motif, which is formed by a neutral THF molecule and two monoanionic BH_4^- ligands for Ln1 (and vice versa for Ln2) in addition to the coordination of the bridging Cht ligand (Figure 2). Although the localization of

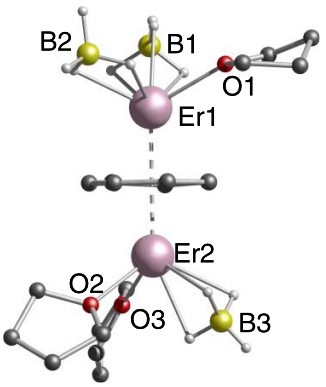

Figure 2. Molecular structure of compound **1-Er** in the solid state. For better clarity, no hydrogen atoms other than the freely refined hydridic hydrogen atoms are shown. Color code: O, red; B, yellow; H, white; C, gray; and Er, pink.

hydrogen atoms bound to heavy metals is difficult, the coordination modes of the BH_4^- ligands could be determined by the free refinement of the hydridic hydrogen atoms. According to this, the two opposite BH_4^- units (B1, B3) are in a η^3-coordination mode, while one, presumably for steric reasons, has a terminal η^2-binding mode (B2), resulting in an increased Ln−B2 distance (e.g., Er1−B2 2.730(5) Å) compared to Ln−B1 and Ln−B3 distances (e.g., Er1−B1 2.524(5) Å, Er2−B3 2.527(5) Å).

Unfortunately, it is not possible to clearly derive the BH_4 binding modes from Raman spectra. In the experimentally obtained Raman spectrum of **1-Y**, the three signals attributable to the B−H stretching vibrations would be in good agreement with a tridentate hydrogen-bridged coordination of the three BH_4 at Y. In the Raman spectrum of **1-Er**, the situation is significantly more complicated due to five signals obtained in this region. However, such a situation does not necessarily speak against triple-bridging coordination.

Haaland and Downs found a similarly complicated situation in combined electron diffraction and vibrational spectroscopic studies of $Zr(BH_4)_4$.[53] Additional signals could result from $^{10}B/^{11}B$ isotopic shifts or due to overtones or combination modes of the B−H stretching modes in the range of 2000−2500 cm^{-1} with the B−H bendings or M−H stretching modes close to 1000−1300 cm^{-1}. In addition, intensifying effects such as Fermi resonances of combination modes with energetically close B−H valence vibrations could occur due to the low molecular symmetry. In order to look at the BH_4 bonding situation from a different perspective, we carried out a quantum chemical DFT calculation on **1-Y** (program system TURBOMOLE, RI-DFT, functional BP86, def2-TZVP for all atoms, true minimum checked by a frequency calculation). According to this calculation, all BH_4 groups are actually triple-bridged to Y (Y−B distances 2.519, 2.520, and 2.532 Å, see the Supporting Information (SI)). However, the difference between the experimentally determined crystal data and the calculated coordination in the (theoretical) gas-phase molecule might be due to packing effects in the crystal.

In general, compounds **1-Ln** exhibit similar binding parameters due to their nearly identical ionic radii of the respective Ln^{III}-cations.[52] The Ln-Ct_{Cht} (Ct = centroid) distances, which range from 1.9119(13) Å for Er2-Ct_{Cht} to 1.9839(4) Å for Y1-Ct_{Cht}, are slightly shorter compared to the reported Nd^{III} analogue.[30] Values of the Ln−Ct_{Cht} distances of structurally related compounds are in a similar range.[34] The 10π-aromatic Cht ligand in **1-Ln** is planar and exhibits a bridging μ−η^7:η^7 mode between the two Ln^{III} cations in a nearly perfectly linear coordination mode (Ln1-Ct_{Cht}-Ln2 angle between 179.03(2)° and 179.27(13)°). In the ^1H NMR spectrum of **1-Y** in THF-d_8 at room temperature, the resonance of the magnetically equivalent ring protons of the aromatic Cht ligand is detected as a singlet at a chemical shift of δ = 5.29 ppm. The hydridic hydrogen atoms of the BH_4^- ligands exhibit a typical splitting into a broad quartet between δ = 0.29 and −0.33 ppm. In addition, signals attributable to coordinating THF are observed. The integral ratios indicate the presence of two remaining molecules of THF per formula unit after the substance was dried *in vacuo*. In the $^{13}C\{^1H\}$ NMR spectrum, the signal of the magnetically equivalent ring carbon atoms of the Cht ligand at δ = 79.5 ppm splits into a triplet, indicating the coupling of two ^{89}Y nuclei with nuclear spin I = 1/2. The coupling constant $^1J_{YC}$ = 2.6 Hz is comparable with the reported values.[54] Moreover, a cross signal of the ring protons with the signal found at δ = −12.0 ppm for ^{89}Y can be observed in the $^1H/^{89}Y$ HMBC spectrum.

The structural motif of compounds **1-Ln** opens the possibility for subsequent functionalization and thus the synthesis of multidecker complexes, due to the presence of apical BH_4^- ligands. To accomplish this, we used 2 equiv of $[K_2(Cot^{TIPS})]$ to introduce the silyl-substituted, eight-membered ring as outer decks in the triple-decker compounds $[(thf)_3K\{(\eta^8\text{-}Cot^{TIPS})Ln^{III}\}_2(\mu\text{-}\eta^7\text{:}\eta^7\text{-}Cht)]$ (**2-Ln**, Ln = Y, Er) (Scheme 1).[51] By recrystallization from hot THF, single crystals of the class **2-Ln** compounds were obtained. Compounds **2-Ln** crystallize in the monoclinic space group $P2_1/m$ with half of a molecule in the asymmetric unit. Figure 3 shows the molecular structures in the solid state. The trianionic Cht ligand in **2-Ln** is present in a μ−η^7:η^7 coordination mode, as also described for starting compounds **1-Ln**. Together with the two outer doubly negatively charged Cot^{TIPS} ligands, each bound to a Ln^{III} cation in a η^8 mode, an anionic lanthanide triple decker is formed. Charge balancing occurs through the potassium cation coordinated to one of the two Cot^{TIPS} ligands in η^8 binding mode. With distances for **2-Er** of Er1-Ct_{Cht} 2.0058(3) Å and Er2-Ct_{Cht} 1.9584(3) Å, the distances of the Ln^{III} cations to the Cht centroid are in a similar range to those of the starting compound **1-Er** and $[KEr_2^{III}(\mu\text{-}\eta^7\text{:}\eta^7\text{-Cht})(N(SiMe_3)_2)_4]$, the only Cht-bridged Er^{III} compound described in the literature.[34] Values in the same range are observed for the Y-Ct_{Cht} distances, leading to Ln−Ln distances of 3.9717(7) Å for **2-Y** and 3.9640(4) Å for **2-Er**. The coordination of the potassium cation to the Cot^{TIPS} ligand (C9−12′) results in slightly shortened Ln2−Ct_{Cht} distances with simultaneously longer Ln2−Ct_{Cot} distances compared to the corresponding distances of the Ln^{III} cation Ln1 (e.g., Er1-Ct_{Cot} 1.8350(3) Å and Er2-Ct_{Cot} 1.8930(3) Å).

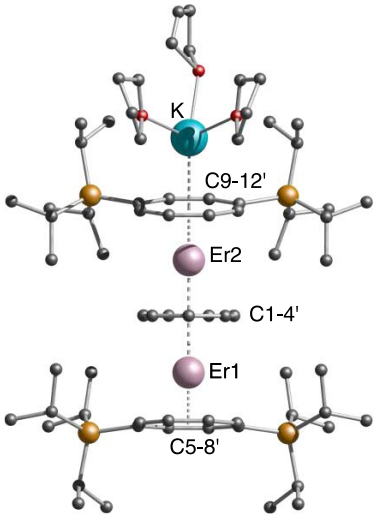

Figure 3. Molecular structure in the solid state of compound class **2-Er**. For better clarity, hydrogen atoms are not shown. Color code: O, red; K, turquoise; Si, orange; C, gray; and Er, pink.

Here, the values for the Ln-Ct_{Cot} distances for both complexes **2-Ln** are in the expected range and agree with the literature data of Cot-based sandwich and multidecker compounds.[19,25,49] As indicated in Figure 3, the triple-decker complexes feature a nearly linear geometry with Ln1-Ct_{Cht}-Ln2 angles of 179.03(2)° (**2-Y**) and 178.719(13)° (**2-Er**) and Ct_{Cht}-Ln2-Ct_{Cot} angles of 172.46(3)° (**2-Y**) and 172.54(2)° (**2-Er**). This bending occurs opposite to the positions of the TIPS substituents and is probably due to their steric demand. The triple-decker motif of **2-Y** was confirmed by two-dimensional $^{1}H/^{89}Y$ HMBC NMR experiments. Cross peaks at a chemical shift of δ = 179.5 ppm in the ^{89}Y NMR with resonances of the ring protons of the seven- (s, δ = 4.11 ppm) and eight-membered rings (two sets of signals, m, δ = 6.21−6.06, δ = 5.91−5.86 ppm) validate the coordination of the Cht and Cot^{TIPS} ligands to the two Y^{III} centers in solution. Moreover, splitting of the signal of the ring carbon atoms of the Cht ligand to a triplet ($^{1}J_{YC}$ = 2.7 Hz) in the $^{13}C\{^{1}H\}$ NMR spectrum can be observed. For the signals of the carbon atoms of the two eight-membered rings, a splitting by $^{1}J_{YC}$ coupling is not resolved. The terminally coordinated potassium cation in **2-Ln** opens the theoretical possibility of synthesizing larger multidecker complexes via a salt elimination reaction. For this purpose, we applied $[Y^{III}(Cot)I(thf)_2]$ as the starting material in the reaction with **2-Y** (Scheme 1). Instead of isolating the anticipated trinuclear quadruple decker, the trianionic Cht ligand was replaced by the dianionic and unsubstituted Cot ligand to exclusively obtain the Cot-based triple decker $[(\eta^8\text{-}Cot^{TIPS}Y^{III})_2(\mu\text{-}\eta^8\text{:}\eta^8\text{-}Cot)]$ (**3**) (Figure 4). The formation of triple-decker complexes featuring two Cot ligands with different substituents in its coordination sphere is unprecedented. To the best of our knowledge, the only heteroleptic Cot-based triple deckers of the rare earth metals are the bis(trimethylsilyl)cyclooctatetraendiide-substituted compounds, $[(\eta^8\text{-}Cot^{1,4\text{-}Me3Si}Ln^{III})_2(\mu\text{-}\eta^8\text{:}\eta^8\text{-}Cot^{1,5\text{-}Me3Si})]$, in which 1,4-$(Me_3Si)_2$-Cot ($COT^{1,4\text{-}Me3Si}$) and 1,5-$(Me_3Si)_2$-Cot ($Cot^{1,5\text{-}Me3Si}$) substituents are present.[25] Homoleptic triple-decker complexes were synthesized in a one-pot reaction, which excludes the selective insertion of two different decks in the triple-decker sandwich complex, e.g., $[Ln_2^{III}(Cot'')_3]$ (Cot" = 1,4-$(Me_3Si)_2C_8H_6$; Ln = Ce, Nd, Sm, Gd, Er) was obtained from $LnCl_3$ and $[Li_2(Cot'')]$.[23,24] In agreement with the structurally related compound $[Y_2^{III}(Cot'')_3]$, the Y-Ct_{C1-8} distance to the silyl-substituted Cot outer deck is 1.7373(3) Å, which is significantly shortened compared to the Y-$Ct_{C9-12'}$ distance to the unsubstituted Cot middle deck with 2.0874(4) Å. Different bond lengths of the Ln atoms to the inner and outer rings were observed earlier, e.g., in $[Nd_2^{III}(Cot'')_3]$.[22] Since bonding in molecular rare earth compounds is mainly electrostatic, the negatively charged central ring interacts with two metal centers and is thus less strongly bonded than the terminal rings. The Ct_{C1-8}-Y-$Ct_{C9-12'}$ angle deviates with 170.03(2)° from the linear coordination.[25] One possible explanation for the preferential formation of Cot-based Y^{III} triple decker **3** instead of the anticipated quadruple decker is the formation of an insoluble coordination polymer of the form $[Y_x^{III}(Cht)_x]$ as a side product. Such poorly soluble coordination polymers with unsubstituted and dianionic Cot ligands are reported for divalent lanthanides.[55−57]

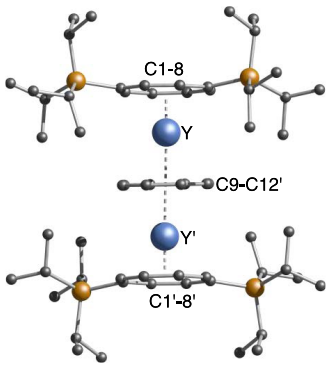

Figure 4. Molecular structure of compound **3** in the solid state. Hydrogen atoms are not shown for the sake of clarity. Color code as in Figure 3 with Y shown in light blue.

Magnetic Behavior. The magnetic characteristic of the **2-Er** complex was investigated via magnetic susceptibility studies. The static magnetic measurements were carried out in a polycrystalline sample of the complex in an applied DC field of 1 kOe. The room temperature $\chi_M T$ value is found to be 21.5 cm^3 K mol^{-1}, which is slightly smaller than expected for two isolated Er^{III} ions, cf., 23 cm^3 K mol^{-1} for two Er^{III} with g_J = 6/5 and J = 15/2. Upon cooling, a gradual decrease of the $\chi_M T$ is observed down to 50 K, where it sharply decreases, reaching an $\chi_M T$ value of 0.39 cm^3 K mol^{-1} at the lowest temperature (2 K) (Figure 5a). The very low $\chi_M T$ at 2 K value is indicative of depopulation of the ligand field levels and/or antiferromagnetic interactions, of dipolar or exchange nature (vide infra). The downturn in the $\chi_M T$ is better rationalized through the $\chi_M(T)$ plot, revealing an upsurge at 25 K followed by a rapid drop at low temperatures (Figure 5a (orange symbols)); this behavior is consistent with antiferromagnetic interactions. Moreover, magnetization studies between 2 and 5 K show a sigmoidal profile (Figure S27), characteristic of a diamagnetic ground state, hence confirming that antiferromagnetic interactions are operative in **2-Er**.

To probe the magnetic anisotropy of **2-Er**, alternating current (AC) magnetic susceptibility studies were conducted. Frequency- and temperature-dependent AC studies under a zero-applied field show the complex to be an SMM (Figures 5c,d and S28). The $\chi''_M(\nu,T)$ reveals a frequency- and temperature-dependent maximum up to 30 K. Below 9 K, the maximum in the $\chi''_M(\nu)$ lies below the experimental

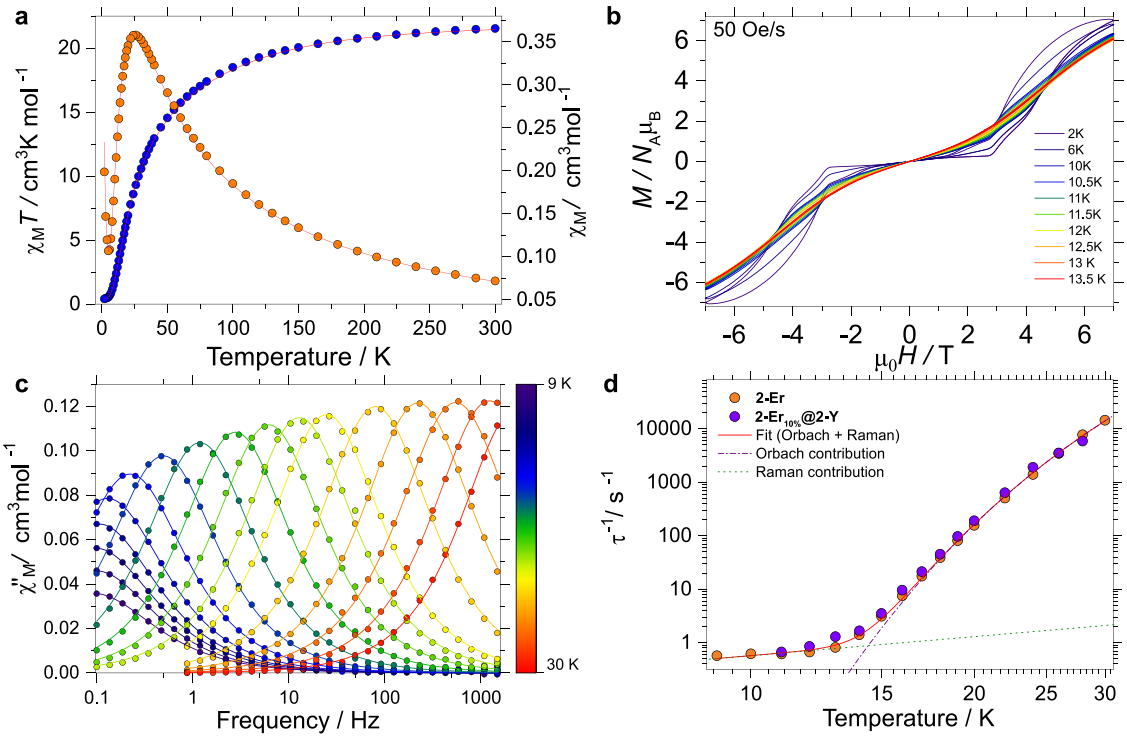

Figure 5. (a) Magnetic susceptibility ($\chi_M T(T)$ and $\chi_M(T)$) data for complexes **2-Er**. The solid traces are fit employing the parameters described in the text; (b) hysteresis loops between 2 and 13.5 K at a sweep rate of 50 Oe/s; (c) temperature-dependent $\chi''_M(\nu,T)$ data with fits (solid lines) employing a generalized Debye model; and (d) $\tau(T)$ data obtained from the Debye analysis for **2-Er** (orange symbols) and the fits to the Orbach and Raman relaxation processes using eq 1 as described in the text. The purple symbols shown in (d) are the relaxation times obtained for the diluted **2-Er$_{10\%}$@2-Y** sample. $\tau(T)$ fits for the **2-Er$_{10\%}$@2-Y** are shown in Figure S29d.

window. Between 9 and 13 K, the maximum shifts slightly, while above 13 K, the maximum strongly becomes temperature-dependent upon increasing temperatures up to 30 K. It is worth pointing out that the $\chi''_M(\nu)$ intensity intensifies upon warming. Attempts to investigate the relaxation dynamics below 9 K via magnetization decay experiments did not yield meaningful results. The $\chi''_M(\nu)$ and $\chi'_M(\nu)$ data of the complex were simultaneously fitted to a generalized Debye model, allowing the extraction of the relaxation times ($\tau(T)$), which were subsequently fitted to

$$\tau^{-1} = \tau_0^{-1} \exp^{-U_{eff}/kT} + CT^n \quad (1)$$

where the first term is the Orbach process and the second is the Raman relaxation process. Fitting of the $\tau(T)$ yields the following parameters $\tau_0 = 9.6(8) \times 10^{-9}$ s, $U_{eff} = 267(2)$ K, $C = 0.04(4)$ s^{-1} K^n, and $n = 1.2(5)$ (Figure 5d). As often observed, the Raman exponent is found to be smaller than expected for Kramer ions.[12,58]

To corroborate that the anisotropic character is of molecular origin, we have performed magnetic dilution studies by doping 10% (molar ratio) of **2-Er** into the diamagnetic **2-Y** analogue, producing **2-Er$_{10\%}$@2-Y** (see the experimental section in the SI for details). AC studies reveal a maximum between 11 and 28 K in the $\chi''_M(\nu)$ data (Figure S29). Plotting the extracted $\tau(T)$ data for **2-Er$_{10\%}$@2-Y** shows a remarkable coincidence between both datasets (Figure 5d orange (**2-Er**) and purple symbols (**2-Er$_{10\%}$@2-Y**)); hence, the magnetic signal can be ascribed to that of diluted **2-Er** into a diamagnetic host (**2-Y**). These results highlight the labile nature of the THF and BH_4 molecules in **1-Ln** and the strong chelating effect of the Cht ligand. Fitting the $\tau(T)$ data of the diluted sample employing eq 1 yields $\tau_0 = 1.98(5) \times 10^{-8}$ s, $U_{eff} = 249(6)$ K, $C = 0.1(5)$ s^{-1} K^n, and $n = 1(2)$ (Figure S29d). The results show that in the temperature range of the study (>11 K), intermolecular interactions do not play an important role in the dynamics of the system. Importantly, the obtained U_{eff} found for **2-Er** is found to be among the highest for Er-Cot-based systems.[8,23,59]

Open hysteresis loops are a definitive proof of the bistable magnetic characteristics of SMMs. To corroborate the SMM character of **2-Er** and the slow relaxation observed through AC studies, magnetization hysteresis loops were collected between 2 and 13.5 K with a sweep rate of 50 Oe/s. Figure 5b shows S-shaped hysteresis loops between 2 and 13.5 K and a field ranging from ±7 T, leading to a blocking temperature (T_B) of 13.5 K (Figure S31). Note that the loops are closed between ±1 T, albeit remaining open above this field range. These characteristics highlight the existence of strong antiferromagnetic coupling operating between the erbium ions in **2-Er**.

In contrast, the hysteresis loop at 2 K of **2-Er$_{10\%}$@2-Y** is open at zero-field (Figure S33), indicating that QTM at the crossings is less effective, and a fraction of spins remain pinned to the excited state (vide infra). This is a direct consequence of the reduced dipolar field nature in the diluted sample, which becomes important below 11 K and will be the subject of further studies.

Electronic Structure Calculations. To comprehend the $\chi_M T(T)$ and $M(H)$ profiles and the low value at the lowest temperature, along with the dynamic characteristic of **2-Er**, CASSCF-SO calculations were performed employing the experimental structure of the complex. The calculations were carried out on the entire molecule substituting one of the Er^{III} ions by Y^{III} at the time (see Section 7 in the SI for details). Expectedly, based on the structural aspects of the molecule, the

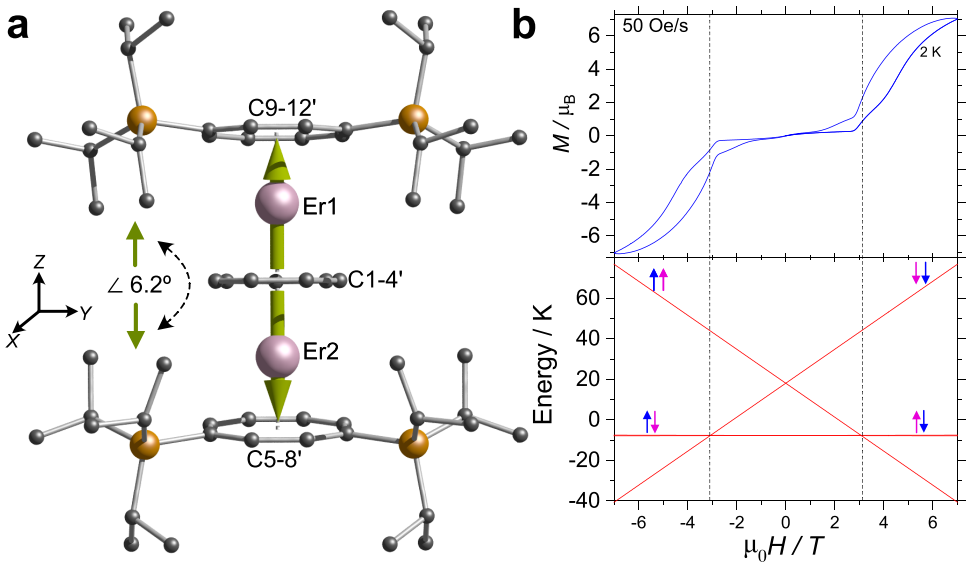

Figure 6. (a) Anisotropy axes (lime arrows) obtained from the CASSCF-SO calculations for **2-Er**. An angle of 6.2° is found between the anisotropy axes of the Er(III) ions via CASSCF calculations. The Er···Er was chosen to lie on the *z*-axis, as depicted. The color code is as in Figure 2. (b) (top) Hysteresis loop at 2 K and (bottom) Zeeman diagram for **2-Er** obtained using eq 2 and parameters described in the text.

CASSCF-SO obtained electronic characteristics for both Er^{III} sites are very similar (Figure 6 and Tables 1 and S9–S11). The

Table 1. CASSCF-SO Calculated Parameters for 2-Er

	Er (1)	Er (2)
GD[a] g_z-values	17.9444	17.9452
GD wave function	99.9%|±15/2>	99.9%|±15/2>
1st excited state/cm^{-1}	214.4	217.7
1st excited wave function	99.4%|±1/2>	99.9%|±1/2>

[a]Ground doublet.

computed effective g_z tensors are 17.9444 and 17.9452 for Er(1) and Er(2), respectively, and are close to the Ising-limit value of 18 characteristics of significant uniaxial anisotropy. The m_J components for the eight lowest Kramer doublets (KDs) of each Er^{III} ion are shown in Tables S9 and S10, respectively. The ground KDs for Er^{III} fragments all predominantly comprised a $m_J = \pm 15/2$ doublet, while the first excited state is $m_J = \pm 1/2$ (Tables S9–S10) and all are highly pure (>95%). The strongly axial character of the ground doublet clearly highlights the strong equatorial ligand field generated by the ligands, which stabilizes well the prolate electronic distribution of Er^{III}.[34] As shown in Figure 6, the anisotropy axes for both ions are practically colinear, with an angle at the Er···Er interconnecting axis of 6.2° (the interconnecting Er···Er lying on the *z*-axis).

The energy barrier of the thermally excited Orbach process relates the energy gap between the ground state and the first excited state, which is found to be 308.4 K (214.4 cm^{-1}) and 313.2 K (217.7 cm^{-1}) (Figure S32). The CASSCF-SO-calculated gap between the ground doublet and the first excited state is of the same order as the barrier obtained via dynamic studies, cf., 267(2) K (186 cm^{-1}) (Tables 1, S9–S10 and Figure S32).

The nearly parallel alignment of the anisotropy axes of the ground doublets in **2-Er** suggests the presence of ferromagnetic dipolar coupling between the ions, which is typically observed for two colinear axes that are also parallel to the interconnecting vector.[60] However, ferromagnetic coupling is in stark contrast to the experimental $\chi_M T(T)$ and $M(H)$ data, clearly indicating antiferromagnetic interactions. The crystal field parameters obtained through CASSCF-SO allow us to quantify the existence of intramolecular interactions operating between the Er^{III} ions. To account for the bimetallic nature of **2-Er**, the Lines model, employing an isotropic exchange between the spin component of the angular momenta of the Er^{III} ions ($S = 3/2$), as implemented in PHI,[61] was used. Hence, the $\chi_M T(T)$ and $M(H)$ were simultaneously fitted employing the following Hamiltonian

$$\mathcal{H}^{i}_{Er} = \mathcal{H}^{i}_{lf} + g_J \mu_0 \mu_B (\hat{J}_{Er(1)} + \hat{J}_{Er(2)}) \boldsymbol{H_z} - 2\boldsymbol{J}^{i}_{\mathbf{lines}} (\hat{S}_{Er(1)} \hat{S}_{Er(2)}) \quad (2)$$

where $\mathcal{H}^{i}_{lf} = \sum_{k=2,4,6,-k\le q\le k} B^q_k O^q_k$ is the ligand field Hamiltonian expressed using Stevens operators, O^q_k are the Stevens operators, B^q_k are the ligand field parameters obtained from CASSCF-SO calculations, $\hat{J}_{Ln}$, $\hat{S}_{Ln}$, and g_J are the spin–orbit, spin-only state, and Landé g-factor for Er^{III}, respectively. Simultaneously fitting the $\chi_M T(T)$ and $M(H)$ employing the crystal field parameters determined from CASSCF-SO and varying solely the exchange interaction result in a $J_{lines} = -2.88(9)$ cm^{-1} ($-12.96(1)$ cm^{-1} projected onto $S_{eff} = 1/2$ for a $-2J$ Hamiltonian) (Figures 5a and S27). Comparison of the Zeeman diagram of the low-lying states with the experimental hysteresis loops shows crossings between the antiferromagnetic ground state and the first excited state occurring at ±3 T (Figure 6b). Note that the best fit requires the inclusion of 2% impurity. This could be a consequence of a small fraction of **2-Er** molecules losing the coordinated THF molecules, hence affecting the local geometry and anisotropy of the affected molecules and/or a small impurity of **1-Er**.

Comparison between the experimentally determined J_{ex} and the dipolar matrix shows that exchange is an order of magnitude stronger than the dipolar interaction, i.e., for an Er···Er distance of 3.9668(4) Å and 6.2° tilting angle between the centers, the strongest dipolar matrix component is

ferromagnetic with J_{zz}^{dip} = +2.236 cm^{-1} (note that the J_{ij}^{dip} is projected on an S_{eff} = 1/2 for a $-J$ Hamiltonian) (see SI Section 6.3). Thus, the exchange interaction plays a major role in the magnetic characteristics of **2-Er**.

At this point and with knowledge of the electronic characteristics of the complexes, it is also possible to rationalize the static and dynamic properties. The SMM character **2-Er** arises from the anisotropic characteristics of the ground doublet states of each Er^{III} ion, which are separated by 308.4 K (214 cm^{-1}) and 313.2 (217.7 cm^{-1}) from the first excited state, respectively. At zero field and for two noninteracting Er^{III} ions, quantum tunneling of the magnetization (QTM) would be active, hence yielding waist-restricted hysteresis loops and a temperature-independent behavior denoted in the $\tau(T)$. Conversely, the strong antiferromagnetic interaction operating between the Er^{III} ions couples both lanthanide ions, leading to a nonmagnetic ground state, as evidenced by the nearly flat hysteresis loops between ±1 T and the first excited-coupled state lying at ∼26 cm^{-1} above it (Figure 6b and Table S13). No SMM behavior would be expected for **2-Er**, due to strong coupling. In contrast, the clear SMM character in **2-Er** implies that the slow relaxation dynamics arise from the thermal population of the first excited coupled-doublet state, as evidenced by the temperature dependence of the isothermal susceptibility (χ_T) obtained by fitting the AC data. The increased population of the excited ferromagnetic state upon warming becomes visible in the AC data (see Figure 5c); hence, the magnetic behavior in **2-Er** can be rationalized as follows: (i) the two Er^{III} ions are connected by an exchange interaction, leading to an antiferromagnetic $|\pm 15/2, \pm 15/2\rangle$ ground state, with the ferromagnetic first excited $|\pm 15/2, \mp 15/2\rangle$ state lying at 25.9 cm^{-1} above it; hence, at low temperatures, no SMM behavior would be expected. The diamagnetic nature of the ground state (<9 K) is reflected in the very weak effect of magnetic dilution observed in (**2-$Er_{10\%}$@2-Y**), as evidenced by the $\tau(T)$ data (Figure 5d); (ii) due to the relatively small separation between the ground and first exchange-coupled excited state, upon warming, the ferromagnetic state becomes populated; hence, the observed slow relaxation dynamics arises from the $|\pm 15/2, \pm 15/2\rangle$; and (iii) relaxation, is therefore, possible between the ferromagnetic state and the second excited state lying at 285.5 K (198.4 cm^{-1}) above the ferromagnetic first excited state. This value bodes well with the experimentally determined barrier (cf., U_{eff} = 249(6) K (173 cm^{-1})). Note that the thermal dependence of the AC data might arise from thermally activated QTM (TA-QTM), providing a plausible explanation for the low Raman component in the $\tau(T)$ analysis. A more detailed investigation of the relaxation characteristics of **2-Er** will be the subject of further studies.

The previously mentioned small angle of 6.2° between the two main magnetic axes is also visible in the $M(H)$ profile, as visible with the small slope of the magnetization curve at fields below 3 T (Figures 5b and S27), with the ground doublet possessing a small magnetic moment of ∼0.96 μ_B. In contrast, the first excited exchange doublet corresponds to the ferromagnetic coupled state, characterized by a large value of the magnetic moment of ∼17.97 μ_B. The step in the $M(H)$ curve at ∼3.0 T is due to QTM occurring at the level crossing of the ground and first excited exchange state doublet (Figure 6).

In a previous study of an erbium−cyclooctatetraendiide triple-decker complex, the strong antiferromagnetic coupling between the Er^{III} ions, with an Er···Er distance of 4.1109(5) Å, was ascribed to be promoted by the delocalized π_z orbitals of the Cot^{2-} ligands. In our work, the central Cot^{2-} was replaced by a Cht^{3-} moiety, leading to a larger interaction as evidenced by the hysteresis loops (crossing at ±3 T, cf., 1.5 T in ref 23). The stronger interaction in our case can be due to a mixture of delocalized π_z orbitals of the Cht^{3-} ligand as well as the shorter Er···Er distance (3.9668(4) Å).

CONCLUSIONS

In summary, we introduced the seven-membered cycloheptatrienyl trianion (Cht) as a bridging unit for the synthesis of the first Cht multidecker complexes. The synthesis of complexes **1-Ln** (Ln = Y, Er) initially extended the variety of Cht-bridged inverse sandwich compounds of the lanthanides. Subsequently, the compounds were used as precursors for synthesizing the triple-decker compounds **2-Ln** via salt metathesis. Compound class **2-Ln** represents the first lanthanide multidecker compounds having a trianionic Cht deck. Moreover, these are also the first rare earth multidecker complexes, which relative to purely carbon-based aromatic ligands are not built up by a bridging Cot derivative. SQUID measurements on the corresponding Er^{III} compound **2-Er** show antiferromagnetic exchange interactions between the two Er^{III} centers. By introduction of the Cot^{TIPS} ligands into the coordination sphere of the Er^{III} ions, the SMM behavior of the compound was significantly improved compared to the only Cht-bridged Er^{III}−SMM to date. As a consequence of the introduction of the Cht^{3-} ligand into the Er^{III} coordination sphere, the largest barrier for an Er-Cot-based triple-decker complex is obtained.[23] Furthermore, the strong interaction between the ions is attained, leading to open hysteresis loops above ±3 T from 2 to 13.5 K, yielding a blocking temperature of 13.5 K. Clearly, Cht^{3-} provides a suitable equatorial ligand field for the enhancement of the magnetic characteristics of Er^{III}-based systems. Furthermore, the presence of a K^+ ion in **2-Ln** would in principle allow swapping it for a lanthanide ion, hence producing magnetic chains. The robust nature of **2-Er** would also permit the synthesis of heteroatomic chains or triple-decker systems for novel technological applications. The reaction of anionic triple-decker **2-Y** with $[Y^{III}(Cot)I(thf)_2]$ resulted in ligand rearrangement and the selective formation of **3**, which is the first triple-decker complex featuring two Cot ligands with different substituents in its coordination sphere.

Accession Codes

CCDC 2303889−2303893 contain the supplementary crystallographic data for this paper. These data can be obtained free of charge via www.ccdc.cam.ac.uk/data_request/cif or by emailing data_request@ccdc.cam.ac.uk or by contacting The Cambridge Crystallographic Data Centre, 12 Union Road, Cambridge CB2 1EZ, U.K.; fax: +44 1223 336033.

AUTHOR INFORMATION

Corresponding Author

Peter W. Roesky − *Institute of Inorganic Chemistry, Karlsruhe Institute of Technology (KIT), D-76131 Karlsruhe, Germany;* orcid.org/0000-0002-0915-3893; Email: roesky@kit.edu

Authors

Adrian Hauser − *Institute of Inorganic Chemistry, Karlsruhe Institute of Technology (KIT), D-76131 Karlsruhe, Germany*

Luca Münzfeld − *Institute of Inorganic Chemistry, Karlsruhe Institute of Technology (KIT), D-76131 Karlsruhe, Germany*

Sören Schlittenhardt − *Institute of Nanotechnology, Karlsruhe Institute of Technology (KIT), D-76344 Eggenstein-Leopoldshafen, Germany*

Cedric Uhlmann − *Institute of Inorganic Chemistry, Karlsruhe Institute of Technology (KIT), D-76131 Karlsruhe, Germany*

Louis Leyen − *Institute of Inorganic Chemistry, Karlsruhe Institute of Technology (KIT), D-76131 Karlsruhe, Germany*

Eufemio Moreno-Pineda − *Facultad de Ciencias Naturales, Exactas y Tecnología, Depto. de Química-Física, Universidad de Panamá, Panamá 0824, Panamá; Facultad de Ciencias Naturales, Exactas y Tecnología, Grupo de Investigación de Materiales, Universidad de Panamá, Panamá 0824, Panamá;* orcid.org/0000-0002-9643-0341

Mario Ruben − *Institute of Nanotechnology, Karlsruhe Institute of Technology (KIT), D-76344 Eggenstein-Leopoldshafen, Germany; Centre Européen de Science Quantique (CESQ), Institut de Science et d'Ingénierie Supramoléculaires (ISIS, UMR 7006), CNRS-Université de Strasbourg, 67083 Strasbourg, France; Institute of Quantum Materials and Technologies (IQMT), Karlsruhe Institute of Technology, 76344 Eggenstein-Leopoldshafen, Germany*

Author Contributions

▽

A.H. and L.M. contributed equally to this work.

Notes

The authors declare no competing financial interest.

ACKNOWLEDGMENTS

The authors gratefully acknowledge support from the Deutsche Forschungsgemeinschaft (DFG, German Research Foundation) through the Collaborative Research Centre "4f for Future" (CRC 1573 project number 471424360, projects B3 and C1) and the Karlsruhe Nano Micro Facility (KNMF, www.kit.edu/knmf) for the provision of access to instruments at their laboratories. Dr. Ralf Köppe is acknowledged for the interpretation of the Raman spectra. The authors acknowledge support by the state of Baden-Württemberg through bwHPC and the German Research Foundation (DFG) through grant no INST 40/575-1 FUGG (JUSTUS 2 cluster).

REFERENCES

(1) Hollemann, A. F.; Wiberg, E.; Wiberg, N. *Lehrbuch der Anorganischen Chemie*; Walter de Gruyter: Berlin, 2007.

(2) Streitwieser, A., Jr; Mueller-Westerhoff, U. Bis-(cyclooctatetraenyl)uranium (uranocene). A new class of sandwich complexes that utilize atomic f orbitals. *J. Am. Chem. Soc.* **1968**, *90*, No. 7364, DOI: 10.1021/ja01028a044.

(3) Greco, A.; Cesca, S.; Bertolini, W. New p-cyclooctateraenyl and p-cyclopentadienyl complexes of cerium. *J. Organomet. Chem.* **1976**, *113*, 321−330.

(4) Streitwieser, A.; Kinsley, S. A.; Jenson, C. H.; Rigsbee, J. T. Synthesis and Properties of Di-π-[8]annulenecerium(IV), Cerocene. *Organometallics* **2004**, *23*, 5169−5175.

(5) Kawasaki, K.; Sugiyama, R.; Tsuji, T.; Iwasa, T.; Tsunoyama, H.; Mizuhata, Y.; Tokitoh, N.; Nakajima, A. A designer ligand field for blue-green luminescence of organoeuropium(II) sandwich complexes with cyclononatetraenyl ligands. *Chem. Commun.* **2017**, *53*, 6557−6560.

(6) Xémard, M.; Zimmer, S.; Cordier, M.; Goudy, V.; Ricard, L.; Clavaguéra, C.; Nocton, G. Lanthanidocenes: Synthesis, Structure, and Bonding of Linear Sandwich Complexes of Lanthanides. *J. Am. Chem. Soc.* **2018**, *140*, 14433−14439.

(7) Jamerson, J. D.; Masino, A. P.; Takats, J. Synthesis of mixed sandwich complexes of the lanthanides, $(\eta^8\text{-}C_8H_8)Ln(\eta^5\text{-}C_5H_5)$. *J. Organomet. Chem.* **1974**, *65*, C33−C36.

(8) Jiang, S.-D.; Wang, B.-W.; Sun, H.-L.; Wang, Z.-M.; Gao, S. An Organometallic Single-Ion Magnet. *J. Am. Chem. Soc.* **2011**, *133*, 4730−4733.

(9) Schumann, H.; Koehn, R. D.; Reier, F. W.; Dietrich, A.; Pickardt, J. Organometallic compounds of the lanthanides. 48. Cyclooctatetraenyl pentamethylcyclopentadienyl derivatives of the rare earths. *Organometallics* **1989**, *8*, 1388−1392.

(10) Münzfeld, L.; Schoo, C.; Bestgen, S.; Moreno-Pineda, E.; Köppe, R.; Ruben, M.; Roesky, P. W. Synthesis, structures and magnetic properties of $[(\eta^9\text{-}C_9H_9)Ln(\eta^8\text{-}C_8H_8)]$ super sandwich complexes. *Nat. Commun.* **2019**, *10*, No. 3135.

(11) Tricoire, M.; Münzfeld, L.; Moutet, J.; Mahieu, N.; La Droitte, L.; Moreno-Pineda, E.; Gendron, F.; Hilgar, J. D.; Rinehart, J. D.; Ruben, M.; Le Guennic, B.; Cador, O.; Roesky, P. W.; Nocton, G. Size-Controlled Hapticity Switching in $[Ln(C_9H_9)(C_8H_8)]$ Sandwiches. *Chem. - Eur. J.* **2021**, *27*, 13558−13567.

(12) Münzfeld, L.; Dahlen, M.; Hauser, A.; Mahieu, N.; Kuppusamy, S. K.; Moutet, J.; Tricoire, M.; Köppe, R.; La Droitte, L.; Cador, O.; Le Guennic, B.; Nocton, G.; Moreno-Pineda, E.; Ruben, M.; Roesky, P. W. Molecular Lanthanide Switches for Magnetism and Photoluminescence. *Angew. Chem., Int. Ed.* **2023**, *62*, No. e202218107, DOI: 10.1002/anie.202218107.

(13) Evans, W. J.; Johnston, M. A.; Greci, M. A.; Ziller, J. W. Synthesis, Structure, and Reactivity of Unsolvated Triple-Decked Bent Metallocenes of Divalent Europium and Ytterbium. *Organometallics* **1999**, *18*, 1460−1464.

(14) DeKock, C. W.; Ely, S. R.; Hopkins, T. E.; Brault, M. A. Preparation, crystal and molecular structure, and properties of an asymmetric lanthanide cyclooctatetraene complex $[Ln(C_8H_8)(OC_4H_8)_2][Ln(C_8H_8)_2]$, where Ln = lanthanum, cerium, neodymium, and erbium. *Inorg. Chem.* **1978**, *17*, 625−631.

(15) Edelmann, A.; Lorenz, V.; Hrib, C. G.; Hilfert, L.; Blaurock, S.; Edelmann, F. T. Steric Effects in Lanthanide Sandwich Complexes Containing Bulky Cyclooctatetraenyl Ligands. *Organometallics* **2013**, *32*, 1435−1444.

(16) Le Roy, J. J.; Jeletic, M.; Gorelsky, S. I.; Korobkov, I.; Ungur, L.; Chibotaru, L. F.; Murugesu, M. An Organometallic Building Block Approach To Produce a Multidecker 4f Single-Molecule Magnet. *J. Am. Chem. Soc.* **2013**, *135*, 3502−3510.

(17) Poremba, P.; Edelmann, F. T. Cyclooctatetraenyl complexes of the early transition metals and lanthanides: X. The first organometallic triple decker sandwich complexes of the lanthanides. *J. Organomet. Chem.* **1998**, *553*, 393−395.

(18) Edelmann, A.; Blaurock, S.; Lorenz, V.; Hilfert, L.; Edelmann, F. T. $[(C_5Me_5)Yb(\mu\text{-}\eta^8,\eta^8\text{-}Cot''')Yb(\mu\text{-}\eta^8,\eta^8\text{-}Cot''')Yb(C_5Me_5)]$—A Unique Tetradecker Sandwich Complex of a Divalent Lanthanide. *Angew. Chem., Int. Ed.* **2007**, *46*, 6732−6734.

(19) Xia, J.; Jin, Z.; Chen, W. Synthesis and crystal structure of a new lanthanide cyclooctatetraene complex $(\eta^8\text{-}C_8H_8)Er(\mu\text{-}\eta^8\text{-}C_8H_8)K(\mu\text{-}\eta^8\text{-}C_8H_8)Er(\mu\text{-}\eta^8\text{-}C_8H_8)K(THF)_4$. *J. Chem. Soc., Chem. Commun.* **1991**, 1214−1215.

(20) Münzfeld, L.; Hauser, A.; Hädinger, P.; Weigend, F.; Roesky, P. W. The Archetypal Homoleptic Lanthanide Quadruple-Decker—Synthesis, Mechanistic Studies, and Quantum Chemical Investigations. *Angew. Chem., Int. Ed.* **2021**, *60*, 24493−24499.
(21) Edelmann, F. T. Multiple-decker sandwich complexes of f-elements. *New J. Chem.* **2011**, *35*, 517−528.
(22) Lorenz, V.; Blaurock, S.; Hrib, C. G.; Edelmann, F. T. The First Linear, Homoleptic Triple-Decker Sandwich Complex of an f-Element: A Molecular Model for Organolanthanide Nanowires. *Organometallics* **2010**, *29*, 4787−4789.
(23) Le Roy, J. J.; Ungur, L.; Korobkov, I.; Chibotaru, L. F.; Murugesu, M. Coupling Strategies to Enhance Single-Molecule Magnet Properties of Erbium−Cyclooctatetraenyl Complexes. *J. Am. Chem. Soc.* **2014**, *136*, 8003−8010.
(24) Poremba, P.; Edelmann, F. T. Cyclooctatetraenyl complexes of the early transition metals and lanthanides: X. The first organometallic triple decker sandwich complexes of the lanthanides. *J. Organomet. Chem.* **1998**, *553*, 393−395.
(25) Lorenz, V.; Liebing, P.; Bathelier, A.; Engelhardt, F.; Maron, L.; Hilfert, L.; Busse, S.; Edelmann, F. T. The "Wanderlust" of Me_3Si groups in rare-earth triple-decker complexes: a combined experimental and computational study. *Chem. Commun.* **2018**, *54*, 10280−10283.
(26) Greenough, J.; Zhou, Z.; Wei, Z.; Petrukhina, M. A. Versatility of cyclooctatetraenyl ligands in rare earth metal complexes of the $[M_2(COT)_3(THF)_2]$ (M = Y and La) type. *Dalton Trans.* **2019**, *48*, 5614−5620.
(27) Münzfeld, L.; Gillhuber, S.; Hauser, A.; Lebedkin, S.; Hädinger, P.; Knöfel, N. D.; Zovko, C.; Gamer, M. T.; Weigend, F.; Kappes, M. M.; Roesky, P. W. Synthesis and properties of cyclic sandwich compounds. *Nature* **2023**, *620*, 92−96.
(28) Miller, J. T.; Dekock, C. W. Facile formation of the cycloheptatrienyl trianion by lanthanide and actinide ions. *J. Organomet. Chem.* **1981**, *216*, 39−48.
(29) Arliguie, T.; Lance, M.; Nierlich, M.; Vigner, J.; Ephritikhine, M. Inverse cycloheptatrienyl sandwich complexes. Crystal structure of $[U(BH_4)_2(OC_4H_8)_5][(BH_4)_3U(\mu\text{-}\eta^7,\eta^7\text{-}C_7H_7)U(BH_4)_3]$. *J. Chem. Soc., Chem. Commun.* **1994**, 847−848.
(30) Arliguie, T.; Lance, M.; Nierlich, M.; Ephritikhine, M. Inverse cycloheptatrienyl sandwich complexes of uranium and neodymium. *J. Chem. Soc., Dalton Trans.* **1997**, 2501−2504.
(31) Arliguie, T.; Lance, M.; Nierlich, M.; Vigner, J.; Ephritikhine, M. Synthesis and crystal structure of $[K(C_{12}H_{24}O_6)][U(\eta\text{-}C_7H_7)_2]$, the first cycloheptatrienyl sandwich compound. *J. Chem. Soc., Chem. Commun.* **1995**, 183−184.
(32) Qiao, Y.; Ganguly, G.; Booth, C. H.; Branson, J. A.; Ditter, A. S.; Lussier, D. J.; Moreau, L. M.; Russo, D. R.; Sergentu, D.-C.; Shuh, D. K.; Sun, T.; Autschbach, J.; Minasian, S. G. Enhanced 5f-δ bonding in $[U(C_7H_7)_2]^-$: C K-edge XAS, magnetism, and ab initio calculations. *Chem. Commun.* **2021**, *57*, 9562−9565.
(33) Huang, W.; Diaconescu, P. L. Rare-earth metal π-complexes of reduced arenes, alkenes, and alkynes: bonding, electronic structure, and comparison with actinides and other electropositive metals. *Dalton Trans.* **2015**, *44*, 15360−15371.
(34) Harriman, K. L. M.; Le Roy, J. J.; Ungur, L.; Holmberg, R. J.; Korobkov, I.; Murugesu, M. Cycloheptatrienyl trianion: an elusive bridge in the search of exchange coupled dinuclear organolanthanide single-molecule magnets. *Chem. Sci.* **2017**, *8*, 231−240.
(35) Lyssenko, K. A.; Antipin, M. Y.; Ketkov, S. Y. Electron density distribution in vanadocene $(\eta^5\text{-}C_5H_5)_2V$ and mixed metallocenes $(\eta^5\text{-}C_5H_5)M(\eta^5\text{-}C_7H_7)$ (M = Ti, V, or Cr) and (η5-C5H5)Ti(η8-C8H8). Effect of the nature of the cyclic ligand on the character of the M−(π-ligand) bond. *Russ. Chem. Bull.* **2001**, *50*, 130−141.
(36) Tamm, M.; Kunst, A.; Bannenberg, T.; Herdtweck, E.; Schmid, R. Cycloheptatrienyl−Cyclopentadienyl−Zirconium Sandwich Complexes: Structure and Bonding. *Organometallics* **2005**, *24*, 3163−3171.
(37) Büschel, S.; Bannenberg, T.; Hrib, C. G.; Glöckner, A.; Jones, P. G.; Tamm, M. Adduct formation of $[(\eta^7\text{-}C_7H_7)Hf(\eta^5\text{-}C_5H_5)]$ with isocyanides, phosphines and N-heterocyclic carbenes: An experimental and theoretical study. *J. Organomet. Chem.* **2009**, *694*, 1244−1250.
(38) Noh, W.; Girolami, G. S. Mono(cycloheptatrienyl) Tantalum Chemistry: Synthesis and Characterization of New Tantalum Halide, Hydride, and Alkyl Species. *Inorg. Chem.* **2008**, *47*, 10682−10691.
(39) Green, M. L. H.; Ng, D. K. P.; Tovey, R. C.; Chernega, A. N. Synthesis and reactions of η-cycloheptatrienyl derivatives of molybdenum. *J. Chem. Soc., Dalton Trans.* **1993**, 3203−3212.
(40) Tamm, M. Synthesis and reactivity of functionalized cycloheptatrienyl−cyclopentadienyl sandwich complexes. *Chem. Commun.* **2008**, 3089−3100.
(41) Glöckner, A.; Bannenberg, T.; Büschel, S.; Daniliuc, C. G.; Jones, P. G.; Tamm, M. Cycloheptatrienyl Zirconium Sandwich Complexes with Lewis Basic Phospholyl Ligands (Phosphatrozircenes): Synthesis, Structure, Bonding and Coordination Chemistry. *Chem. - Eur. J.* **2011**, *17*, 6118−6128.
(42) Glöckner, A.; Cui, P.; Chen, Y.; Daniliuc, C. G.; Jones, P. G.; Tamm, M. Boratatrozircenes: cycloheptatrienyl zirconium boratabenzene sandwich complexes − evaluation of potential η^6−η^5 hapticity interconversions. *New J. Chem.* **2012**, *36*, 1392−1398.
(43) Glöckner, A.; Tamm, M. The organometallic chemistry of cycloheptatrienyl zirconium complexes. *Chem. Soc. Rev.* **2013**, *42*, 128−142.
(44) Green, M. L. H.; Ng, D. K. Cycloheptatriene and-enyl complexes of the early transition metals. *Chem. Rev.* **1995**, *95*, 439−473.
(45) Hilgar, J. D.; Flores, B. S.; Rinehart, J. D. Ferromagnetic coupling in a chloride-bridged erbium single-molecule magnet. *Chem. Commun.* **2017**, *53*, 7322−7324.
(46) Ungur, L.; Le Roy, J. J.; Korobkov, I.; Murugesu, M.; Chibotaru, L. F. Fine-tuning the Local Symmetry to Attain Record Blocking Temperature and Magnetic Remanence in a Single-Ion Magnet. *Angew. Chem., Int. Ed.* **2014**, *53*, 4413−4417.
(47) Hilgar, J. D.; Bernbeck, M. G.; Rinehart, J. D. Million-fold Relaxation Time Enhancement across a Series of Phosphino-Supported Erbium Single-Molecule Magnets. *J. Am. Chem. Soc.* **2019**, *141*, 1913−1917.
(48) Le Roy, J. J.; Korobkov, I.; Murugesu, M. A sandwich complex with axial symmetry for harnessing the anisotropy in a prolate erbium(III) ion. *Chem. Commun.* **2014**, *50*, 1602−1604.
(49) Meihaus, K. R.; Long, J. R. Magnetic Blocking at 10 K and a Dipolar-Mediated Avalanche in Salts of the Bis(η8-cyclooctatetraenide) Complex $[Er(COT)_2]^-$. *J. Am. Chem. Soc.* **2013**, *135*, 17952−17957.
(50) Rinehart, J. D.; Long, J. R. Exploiting single-ion anisotropy in the design of f-element single-molecule magnets. *Chem. Sci.* **2011**, *2*, 2078−2085.
(51) Hauser, A. *Dissertation, Karlsruher Institut für Technologie (KIT): Aktivierung von Elementen der Gruppe 15 sowie Darstellung neuer Lanthanoid-Sandwichverbindungen*; Cuvillier Verlag Göttingen, 2023.
(52) Shannon, R. D. Revised effective ionic radii and systematic studies of interatomic distances in halides and chalcogenides. *Acta Crystallogr., Sect. A* **1976**, *32*, 751−767.
(53) Haaland, A.; Shorokhov, D. J.; Tutukin, A. V.; Volden, H. V.; Swang, O.; McGrady, G. S.; Kaltsoyannis, N.; Downs, A. J.; Tang, C. Y.; Turner, J. F. C. Molecular Structures of Two Metal Tetrakis(tetrahydroborates), $Zr(BH_4)_4$ and $U(BH_4)_4$: Equilibrium Conformations and Barriers to Internal Rotation of the Triply Bridging BH_4 Groups. *Inorg. Chem.* **2002**, *41*, 6646−6655.
(54) Schumann, H.; Winterfeld, J.; Glanz, M.; Köhn, R. D.; Hemling, H. Metallorganische verbindungen der lanthanoide: LXXXV1184. Mitteilung siehe Lit. 1.. Synthese und strukturaufklärung neuer cyclooctatetraenyl-cyclopentadienyl-sandwich-komplexe der seltenen erden. *J. Organomet. Chem.* **1994**, *481*, 275−282.
(55) Hayes, R. G.; Thomas, J. L. Synthesis of cyclooctatetraenyleuropium and cyclooctatetraenylytterbium. *J. Am. Chem. Soc.* **1969**, *91*, No. 6876, DOI: 10.1021/ja01052a070.

(56) Huttmann, F.; Schleheck, N.; Atodiresei, N.; Michely, T. On-Surface Synthesis of Sandwich Molecular Nanowires on Graphene. *J. Am. Chem. Soc.* **2017**, *139*, 9895−9900.
(57) Wayda, A. L.; Cheng, S.; Mukerji, I. Cyclooctatetraenide derivatives of divalent samarium. *J. Organomet. Chem.* **1987**, *330*, C17−C19.
(58) Goodwin, C. A. P.; Reta, D.; Ortu, F.; Chilton, N. F.; Mills, D. P. Synthesis and Electronic Structures of Heavy Lanthanide Metallocenium Cations. *J. Am. Chem. Soc.* **2017**, *139*, 18714−18724.
(59) Meng, Y.-S.; Wang, C.-H.; Zhang, Y.-Q.; Leng, X.-B.; Wang, B.-W.; Chen, Y.-F.; Gao, S. (Boratabenzene)(cyclooctatetraenyl) lanthanide complexes: a new type of organometallic single-ion magnet. *Inorg. Chem. Front.* **2016**, *3*, 828−835.
(60) Bernbeck, M. G.; Orlova, A. P.; Hilgar, J. D.; Gembicky, M.; Ozerov, M.; Rinehart, J. D. Dipolar Coupling as a Mechanism for Fine Control of Magnetic States in ErCOT-Alkyl Molecular Magnets. *J. Am. Chem. Soc.* **2024**, *146*, 7243−7256.
(61) Chilton, N. F.; Anderson, R. P.; Turner, L. D.; Soncini, A.; Murray, K. S. PHI: A powerful new program for the analysis of anisotropic monomeric and exchange-coupled polynuclear d- and f-block complexes. *J. Comput. Chem.* **2013**, *34*, 1164−1175.